



HAL
open science

Observation of a modified superficial layer on heavily loaded contacts under grease lubrication

L. Frache, E. Houara Komba, D. Philippon, J. Galipaud, M.I. de Barros, Thierry Douillard, K. Masenelli-Varlot, N. Bouscharain, Y. Maheo, R. Sarlin, et al.

► **To cite this version:**

L. Frache, E. Houara Komba, D. Philippon, J. Galipaud, M.I. de Barros, et al.. Observation of a modified superficial layer on heavily loaded contacts under grease lubrication. Tribology International, 2021, 158, pp.106921. 10.1016/j.triboint.2021.106921 . hal-03155000

HAL Id: hal-03155000

<https://hal.science/hal-03155000>

Submitted on 13 Feb 2023

HAL is a multi-disciplinary open access archive for the deposit and dissemination of scientific research documents, whether they are published or not. The documents may come from teaching and research institutions in France or abroad, or from public or private research centers.

L'archive ouverte pluridisciplinaire **HAL**, est destinée au dépôt et à la diffusion de documents scientifiques de niveau recherche, publiés ou non, émanant des établissements d'enseignement et de recherche français ou étrangers, des laboratoires publics ou privés.



Distributed under a Creative Commons Attribution - NonCommercial 4.0 International License

OBSERVATION OF A MODIFIED SUPERFICIAL LAYER ON HEAVILY LOADED CONTACTS UNDER GREASE LUBRICATION

L. Frache^{a,b,*}, E. Houara Komba^{a,b}, D. Philippon^a, J. Galipaud^{d,e}, M.I De Barros^d, T. Douillard^e, K. Masenelli-Varlot^e, N. Bouscharain^a, Y. Maheo^b, R. Sarlin^b, G. Le Jeune^b, Y. Berthier^a, B. Bou-Said^a, F. Massi^{a,c}

^a Univ Lyon, CNRS, INSA-Lyon, LaMCoS, UMR5259, F-69621 Villeurbanne, France

^b SKF Aerospace, 22 rue Brillat Savarin, CS 16235, 26958, Cedex 9, Valence, France

^c University of Rome 'La Sapienza', Department of Mechanical and Aerospace Engineering, via Eudossiana 18, 00184 Rome, Italy

^d Univ. Lyon, Ecole Centrale de Lyon, LTDS, 36, Av Guy de Collongue, Ecully Cedex 69134, France

^e Univ. Lyon, INSA-Lyon, Université Claude Bernard Lyon 1, MATEIS, UMR 5510, CNRS, 7 avenue Jean Capelle, F-69621, Villeurbanne Cedex, France

*Corresponding author: lucas.frache@insa-lyon.fr (L. Frache)

Abstract

Several industrial applications require bearings to work under slow oscillating motions and very high contact pressures (aircraft actuators, wind turbine, robotic arms, etc.). Hence, a boundary lubrication regime predominates. However, grease provides the lubrication essential to assure bearing integrity. In this study, the mechanisms involved in protecting the contact surfaces are investigated. High loaded oscillating movements have been applied on a commercial greased deep groove ball bearing. The morphology of its contact was observed using Scanning Electron Microscopy (SEM), revealing superficial transformations. Further, with an extreme surface X-Ray Photoelectron Spectroscopy (XPS) analysis, three cross-sections made by a nanomachining process (FIB) were investigated using Transmission Electron Microscopy (TEM). The analyses revealed a modified layer at the contacts generated by grease interactions.

Keywords

Grease, High loaded bearings, Oscillating bearings, Modified layer, Tribofilm

1. Introduction

Because of the high power to be transmitted, many applications require localized contact interfaces (gears, bearings, cams, etc.) working above the yield stress of materials (1,2). Actuator bearings in wind turbines or aeronautics are often used to operate high aerodynamic forces, leading to contact pressures of several GPa. Those components are dedicated to adjust the position of the blades, aileron, robotic arms, among others. Because such displacements result in small oscillations at low speed, a grease lubrication is generally used to provide oil and additives with a dedicated thickener at the contact.

Combination of high contact pressures and oscillating movement, which induces transitory phases, prevents a full lubricant fluid film formation to spread along the contact surfaces. However, experiments have proved that grease is essential for operating the bearing (1,2). Thus, a more complex lubrication mechanism, involving lubricant additives, is required in such operative mixed/boundary conditions.

Lubricated continuous rolling bearings have been widely investigated. Many studies about fatigue in the elastohydrodynamic lubrication (EHL) regime have shown competition between wear modes during a bearing life-cycle (3,4). Theoretically, subsurface fatigue is the main failure of bearings in the EHL regime (5). However, small modifications in the tribological triplet (6) commonly lead to other wear mechanisms. For instance, surface irregularities of the first bodies generate high local contact pressures, inducing local steel-steel contacts and mild wear (7). Mild wear can positively affect surface shapes, but can generate wear particles in the third body that lead to surface indentations (3,8), and eventually to surface crack initiation (9). There is a constant competition between these accommodation mechanisms, therefore models have to include such a wide range of wear phenomena (10).

When plasticity is introduced, because of very high contact pressures, the commonly used Hertzian model has not been adapted for the prediction of contact stresses and strains (11). Several approaches have been developed to predict the bearing lifetime (12): phenomenological engineering, finite element simulations based on heavy material laws, and semi-analytical. In these models, rolling contact fatigue has application-specific behaviors, and a barrier to develop a reliable model strongly depends on understanding the running-in stage and the interaction between wear and lubricant in the plasticized contact (13). A good surface protection, leading to a reduced friction coefficient, enables crack initiation in the subsurface and propagation in V

shape for rotational bearings (14). The propagation stage can amount to 40% of the bearing lifetime (15). It is therefore important to manage the surface evolution, strongly dependent on the lubricant capabilities.

While high loaded oscillating bearings are becoming a major concern in industrial applications (16), few studies directly address the tribological analysis of such particular working conditions. Recent studies reproduced and described the life-cycle scenario for greased deep groove ball bearings (2,17) and greased single row roller bearings (18), using the same operative conditions and materials. In both damage evolution scenarios, five common phases have been identified:

- Running-in: micro and macro modifications of the surface topography.
- Steady state: no observable surface degradation, constant resistant torque.
- Damage initiation: noticeable fast degradation of the contact surfaces.
- (Potential second steady state if the contact accommodates with the new surface state).
- Damage growth: accumulation of degradations leading to the bearing end of life.

If the geometry (either ball or roller bearing) does not modify the main phases of the degradation scenario, it has an important impact on determining the component where failure initiates—the ball for the deep groove ball bearing (2,19) and the inner ring for the single row roller bearing (18). However, in both cases, a sudden detachment of superficial material occurs, which is a common failure mode of a high loaded rotational bearing with well-protected surfaces. Moreover, for both geometries, the main lifetime of the bearing is characterized by a long steady state, where no relevant signs of degradation are observed at the contact surfaces (2,17,18). The observations and results assume that, despite the lack of a stable lubricant fluid film at the contact because of specific boundary conditions (low speed and high load), the lubricating grease protects the surfaces from steel-steel interactions, which would lead to superficial and fast wear (2).

Therefore, this study investigated the surface and interface accommodation mechanisms, which prevent large superficial wear along the steady state of the bearing life-cycles.

Several high strain and stress condition surface and interface mechanisms have been described, with various lubrications used. Whenever localized contacts undergo high stress and gradients

(rail-wheel, roller-race, gear teeth, etc.), thermo-mechanical actions bring a transformation of the surface and/or subsurface layer of the materials in contact. The modified region is then called the tribologically transformed structure (TTS) (20,21). A TTS is defined as a modification of the material of the solids in contact, either in surface or subsurface, including phase transformations or grain refinement up to the nanometric scale (21,22).

Moreover, in high strain and stress conditions, chemical superficial films have been observed (23,24). They are due to the tribochemical reaction of the lubricant additives with free chemical bonds at the extreme surface activated by metal-metal contacts (23,25), and with the chemical environment activated by high temperature (26). The coupled mechanical and thermal stresses originate at the formation of this nanometric layer on the contact surface. Despite its superficial aspect, this layer (often referred as tribofilm) enhances contact capabilities like wear reduction (25,27) and load carrying capacities (28).

When considering high loaded greased contacts, a key role in contact surfaces and interfaces conditioning is played by the additives, in particular EP (extreme pressure) and AW (anti-wear) additives. EP additives were based on reactive compounds containing lead (Pb), sulfur (S) and phosphorous (P), or combinations (29). Nevertheless, in the mid-90s, lead had to be removed from lubricants for environmental and health reasons. Therefore, phosphorous-sulfur additives were tried, but with poor results for extreme working conditions (30). However, researchers lead was replaced with other metals; bismuth (Bi) has been selected and appears well-suited to react with sulfur and phosphorous, to protect surfaces (28,29).

Other additives have been investigated to operate in EP conditions, like calcium carbonate (31) or zinc dithiophosphate (ZnDDP) (23), and have shown good abilities to protect contact surfaces from superficial wear. Those additives have been extensively investigated (32), (33) and are common in commercial EP and AW additive packages.

In previous studies on the observed bearings (2,17,18), despite an oil starvation, the contact surface topography of the rolling elements and raceways remain stable after running-in, and maintained a steady state until bearing failure initiation. Thus, in this study, we investigate the physico-chemical and structural evolution of the contact surfaces, which allows the heavily loaded interface accommodation resulting in contact protection. First, we will overlook the experimental conditions, to reproduce and observe the life-cycle of high loaded oscillating bearings. Then, considering the studies conducted on deep groove ball bearings (2), (17), a

representative bearing specimen will be investigated, and the morphology of the contact surface analyzed. To determine the chemical composition of the contact surface, XPS is conducted, whereas Transmission Electron Microscopy (TEM) on FIB cross-sections investigates the surface and subsurface morphology of different contact zones. This multi-technique approach highlights the formation of a protective modified layer at the contact interface.

2. Materials and methods

A large campaign of endurance tests on high loaded oscillating ball bearings have been developed in [2][5], following the evolution of the contact surface topography during the different bearing life phases. Here, a bearing sample, representative of that endurance campaign, will be investigated in depth to highlight the morphology and transformations at the contact surfaces during the steady state of the bearing life.

2.1. Experimental setup

The experimental tests are conducted on a commercial deep groove ball bearing, made of high carbon steel 100Cr6 (AISI 52100), whose physical and mechanical properties are summarized in Table 1. Thanks to its hardness and toughness, this material is used for applications such as bearings and industrial tools as it is well adapted to resist against wear and fatigue aging.

Mechanical properties	Steel 100Cr6 (AISI52100)
Coating	No
Heat treatments	Hardened and tempered
Density [g/cm ³]	7.9
Hardness	HRC 60/63
Modulus of elasticity [GPa]	210
Yield stress σ_E [GPa]	1.1

Table 1: Material properties of steel 100Cr6 from SKF Aerospace

To match with real operating conditions, the lubricant used here is the Aeroshell Grease 33, approved for the aviation field. This lubricant is a formulated grease with a lithium and calcium complex thickener (Table 2), with a synthetic base oil and additives package. Its load carrying, corrosion, and oxidation additives make it suitable for a wide range of applications on aircrafts, which allow standardize routine lubrications (34). The Aeroshell Grease 33 is used for aileron actuators, which involve high load oscillating movements. For the grease application, the bearing is filled at 100% before the test, rotating the bearing rings to provide a homogeneous distribution between the rollers and raceways.

Commercial appellation	Aeroshell Grease 33	
Thickener type	Li & Ca complex	
Oil type	Synthetic Hydrocarbon & Ester	
Base oil viscosity [mm²/s]	@ -40°C	1 840
	@ 40°C	14,2
	@ 100°C	3,2
Temperature range	-73 to 121 °C	
Dropping point	216 °C	

Table 2: Aeroshell Grease 33 properties

The experimental endurance tests are performed on the SKF test bench "R2" (Figure 1), dedicated to replicate the working conditions of such high loaded oscillating bearings.

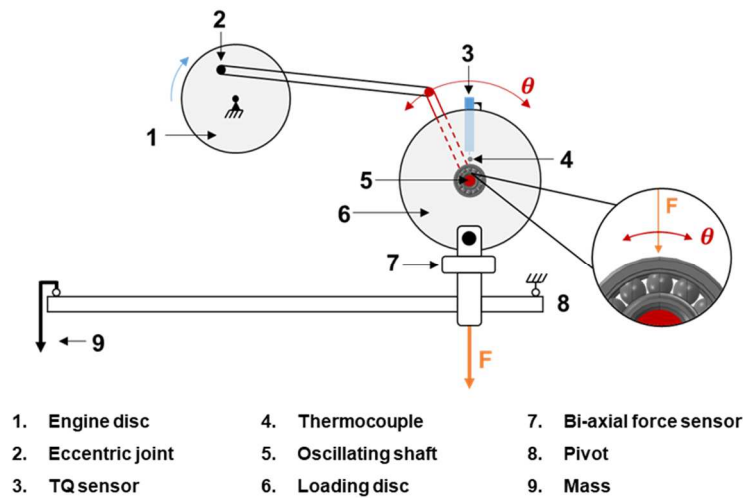


Figure 1: Scheme of the "R2" test bench

Bearing type	Deep groove ball bearing
Bearing material	100Cr6 (AISI52100)
Lubricant	Aeroshell Grease 33
Level of lubrication	Full
Radial load (F)	10,800 N
Oscillation amplitude	+/- 20°
Oscillation frequency	5 Hz
Modulus of elasticity [kN/mm²]	210

Table 3: Experimental test conditions on the deep groove ball bearing sample

The "R2" test bench enables the application of oscillating motion and high loads for several bearing designs. The bearing is first inserted in the household of the loading disc (Figure 1, (6); Loading disc). Then, the assembly is mounted on the oscillating shaft (Figure 1, (5); Oscillating shaft), which is respectively fixed with the inner ring. The load is applied on the loading disc thanks to a lever arm system (Figure 1, (7)/(8)/(9)) and dead weights. The shaft oscillates because of the electric engine and crank-rod kinematic system. Therefore, the inner ring

oscillates while the outer ring is fixed with the loaded disk. The controlled input parameters are the oscillation amplitude, frequency, and radial load. The output variables, recorded by a modular acquisition system (OROS-OR36), are the relative radial displacement (RD) between the inner ring and the outer ring, the temperature on the external surface of the outer ring, the radial load, and the resistant torque (RT) of the bearing. The load and the RT are measured with a bi-axial force transducer. The “R2” setup is detailed in the work dedicated to establish the life evolution of high loaded oscillating bearings (2).

For the analysis, the conditions of the test are the same used for establishing the degradation scenario of the deep groove ball bearing (2). The radial load applied on the bearing is 10,800 N, which allows the setup to reach a maximum contact pressure of 4 GPa at the most loaded contact interface, derived from the 3D elastoplastic finite element simulation (19). The oscillation amplitude is fixed at $\pm 20^\circ$ to avoid fretting domain between 0° and the dither angle (2), without resulting in an overlapping of the rolling surfaces of the balls. The frequency is fixed to 5 Hz to minimize the test duration and avoid overheating; the test conditions are listed in Table 3.

2.2. Surface analysis

Previous studies on high loaded oscillating bearings have shown that the Aeroshell Grease 33 protects contact surfaces (2), (17). This ensures a long lifetime, until a macroscopic detachment of material occurs, either on the ball for the deep groove ball bearing (2), (17), or on the inner ring raceway for the roller bearing (18). In fact, a long steady state period, with no relevant degradation of the surfaces, has been observed on the bearing life evolution curve (Figure 2). However, such operating conditions (mixed/boundary) prevent any oil film formation between surfaces. Preliminary observations (2), (17) of the contact surfaces showed a smooth superficial layer at the raceway surface, in the zones where higher stresses and local sliding are expected. During those studies, at least 64 bearings were tested and 15 bearings were observed using Scanning Electron Microscopy (SEM). This study aimed to provide a deep investigation of the surfaces in contact, to identify the presence and morphology of such modified layer, which is formed in the presence of grease and which protects the surfaces.

To investigate this phenomenon, a deep groove ball bearing was prepared on the “R2” setup. The test was stopped during the steady state (Figure 2) of the bearing life, when both the RT and the RD remain stable (2).

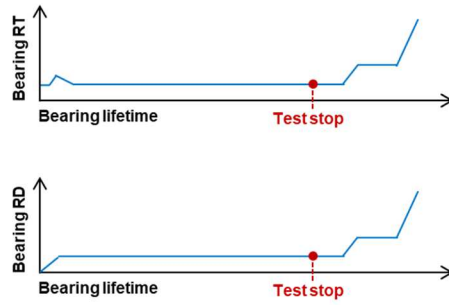


Figure 2: Positioning of the test interruption for the bearing analysis on the wear model of the high loaded oscillating deep groove ball bearing (2)

Using SEM, an overall observation of the contact zones was conducted (FEI Quanta 600 operating at 15 kV, spot 5, and equipped with a Secondary Electron Everhardt-Thornley detector). In previous studies, dedicated to the analysis of the bearing life-cycle under those conditions (2), (17), SEM observations showed the inner ring surface and ball surface remained undamaged during the steady-state phase. This suggests that the third body's (grease and wear particles) interaction with the surfaces provides a good protection against superficial wear along the steady state.

Figure 3 shows the observations focused on the most loaded contact pairs, comprising the ball B1 and the corresponding trace on the inner ring T1, with their neighbor pair B2 and T2. It was observed that despite possible local sliding, the rolling elements remain within their theoretical calculated rolling traces of 1.6 mm for an oscillation amplitude θ of 40° . The suffixes “-b” (border) and “-c” (center) were used to localize investigated areas on the trace. The load distribution on the balls along the oscillation are also presented in Figure 3. The initial positions of the balls are $B1_{t0}$ and $B2_{t0}$ for B1 and B2, respectively. The maximum radial load was reached by the B1-T1 pair (about 3,900 N).

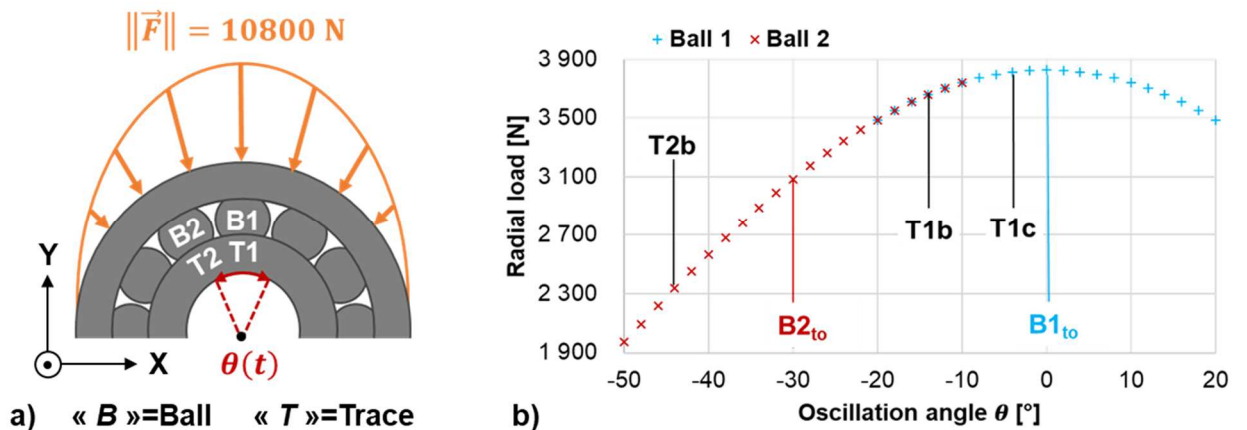


Figure 3: High loaded oscillating bearing test setup. a) Elements definition and b) load distribution on the most loaded ball and the adjacent one.

The investigation focused on the inner ring raceway, where the maximum pressures are reached and where the rolling traces are identified. SEM observations reveal different morphologies of the surface depending on the contact zone (Figure 4). Previous studies [2][5][6][15] have shown how zones can be identified where higher local sliding is expected. They were located at the border of each single trace on the raceway where the respective rolling element inverses its direction. In such areas, an accumulation of a third body has been observed.

With these considerations, the surfaces of interest were first cleaned, to remove the residual grease and detached worn particles, using the following procedure: 5 minutes sonication in acetone (99.8% purity), followed by 5 minutes sonication in heptane (98% purity) and then 5 minutes sonication in acetone. The following zones (Figure 4) of the overall contact surfaces were studied:

- Trace 1 border (T1b): located in T1. This is a reverse point of B1, where the ball changes its rolling direction. Because of the transient phase, a more important sliding ratio is expected, resulting in a higher shearing of the third body regarding the rest of the rolling trace T1. Before the cleaning protocol, an accumulation of the third body is observed here. In this zone, a smooth superficial layer is observed (Figure 4).
- Trace 1 center (T1c): located in T1. This area is closer to the center of the T1 rolling trace, where rolling motion predominates. Machining grooves are visible on SEM observations T1c and their plastic deformation is evidenced (Figure 4).
- Trace 2 border (T2b): located in T2 at a reverse point of B2. Because of the lower load, and its direction, regarding T1b (Figure 3), the sliding ratio is higher at this zone. For the same reason than T1b, a third body accumulation is observed before the washing. SEM observations of T1c show a well-constituted smooth superficial layer (Figure 4).

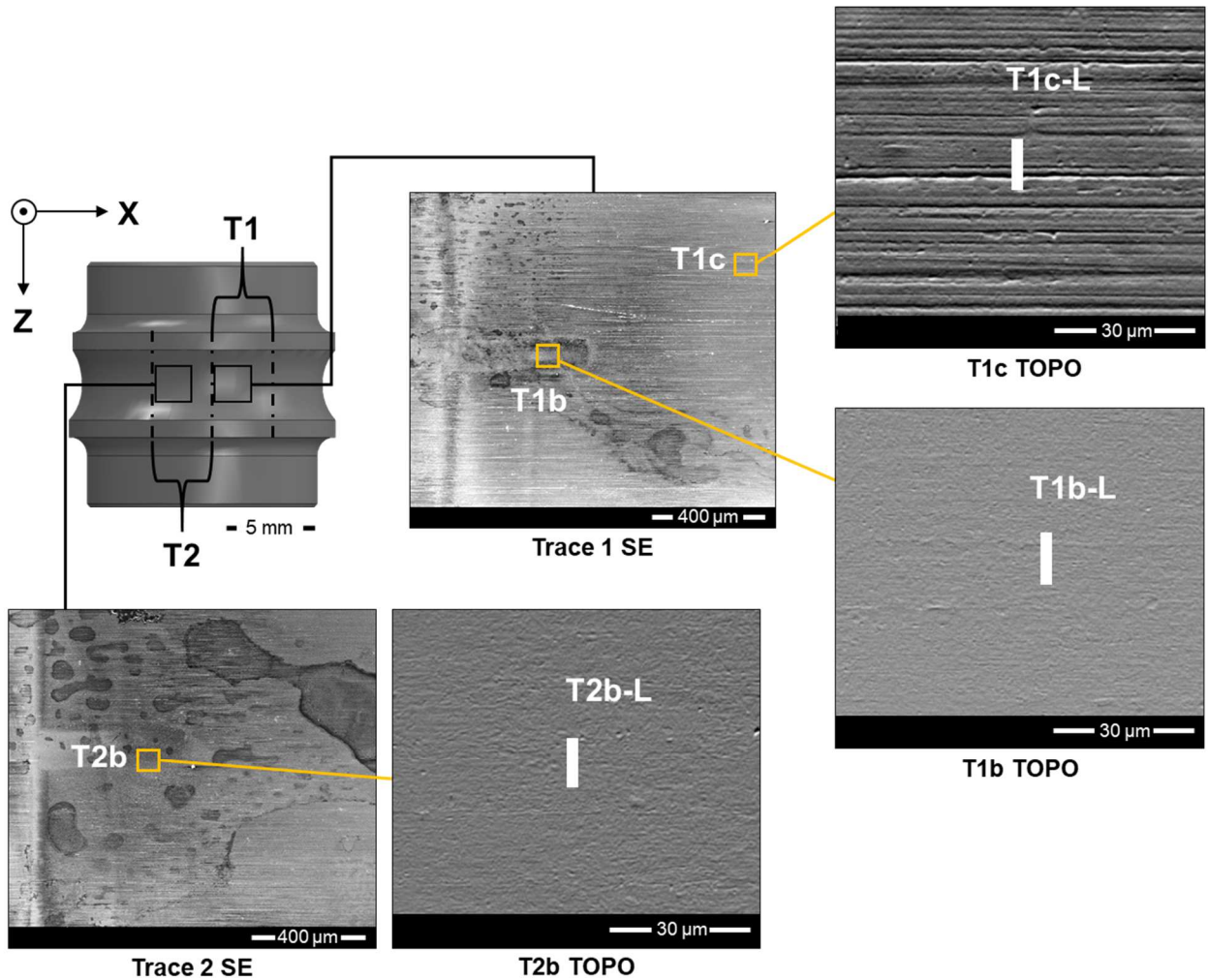


Figure 4: SEM (tension 15 keV, spot 5, WD 10.8 mm) observations of the rolling traces T1 and T2. The magnifications show details of the smoothed superficial layer at the reversing areas T1b and T2b; another magnification shows a detail of the plasticized area T1c at the central zone of the contact trace.

These SEM observations agree with previous analyses on both the deep groove ball bearing (2) and the single row roller bearing (17). They reveal smooth areas close to the reversing points, with same topography and localization.

2.3. Analysis protocol

An X-Ray Photoelectron Spectroscopy (XPS) analysis was performed to identify the elements in the areas observed by SEM microscopy (Figure 4). An ULVAC-PHI Versaprobe II spectrometer, equipped with a monochromatized Al K α (1,486.6 eV) source, was used. Survey spectra were taken at a 187-eV pass energy, with an energy resolution of 0.8 eV/step. A spot size of 50 μm was used in all analyses and a depth observation of ca. A 10 nm depth resolution can be considered. To prevent any differential charging effect, the sample was electrically insulated, and a dual beam neutralizer was used for charge compensation. The spectra were calibrated using the C 1s transition at 284.8 eV. Because the aim of this analysis is to identify a modified

layer, constituted by the interaction between grease and bearing steel, the survey spectra will reveal grease elements on the surface.

A Dual Beam SEM/FIB FEI Helios 600i was used for nanomachining three lamellae using an ion beam of gallium Ga⁺. The lamellae are cross-sections of the inner ring localized in the areas T1b, T1c, and T2b and are referred as T1b-L, T1c-L, and T2b-L, respectively (Figure 4). Before the nanomachining process on the inner ring surface, two thin platinum layers were deposited to prevent damage by the gallium beam on the selected contact areas.

Once the lamellae were obtained, TEM observations were performed on a JEOL 2010F microscope operating at 200 kV. Bright field images were acquired with a Gatan Orius 100 CCD camera.

3. Identification of the modified superficial layer

3.1. XPS analysis

XPS spectra are presented in Figure 5 for each identified area, T1b, T1c, and T2b, and have similar profiles. Despite the heavy cleaning described in section 2.2 *Surface analysis*, they all reveal iron, oxygen, carbon, calcium, sulfur, bismuth, and phosphorous on the surface of the inner ring raceway.

According to the steel 100Cr6 composition (Table 4), it contains neither calcium nor bismuth elements, and the pollutants based on sulfur and phosphorous are too negligible to be detected. The iron in the steel 100Cr6 is barely detected by the XPS superficial measurements (Figure 5), whereas a mass concentration higher than 95.8% characterizes the alloy.

These considerations assume that a superficial layer may cover the inner ring steel surface. This layer is an aggregation of compounds including oxygen, carbon, bismuth, calcium, phosphorous, and sulfur. Furthermore, these elements unveil the capability for the grease to form a detectable superficial layer.

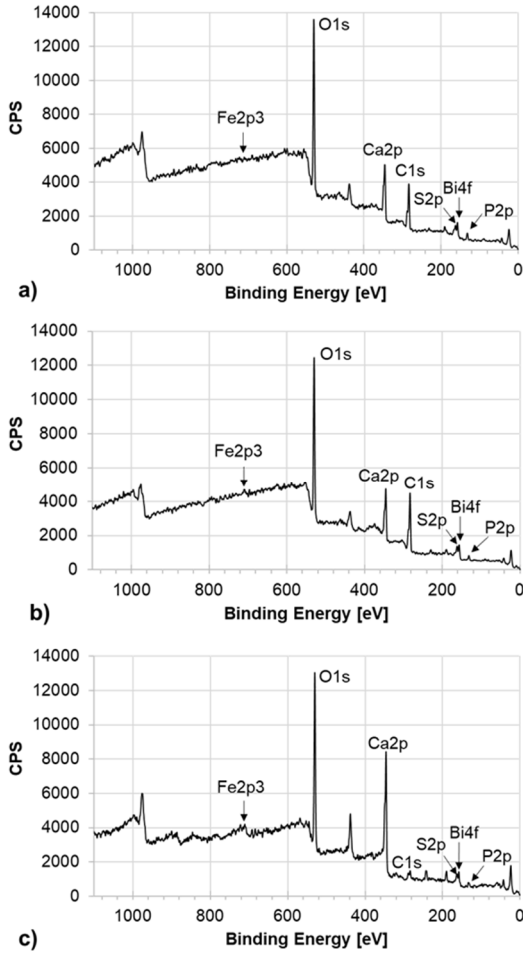


Figure 5: XPS general spectra in spotted area a)T1b, b)T1c, c)T2b.

Steel 100Cr6 (AISI52100)	
Elements	[%(m/m)]
Cr	1.35 - 1.60
C	0.95 - 1.05
Si	0.15 - 0.35
Mn	0.25 - 0.45
P	0.025 ≤
S	0.015 ≤
Mo	0.10 ≤
Al	0.050 ≤
Cu	0.30 ≤

Table 4: ISO 683-17 chemical requirements for Steel AISI 52100

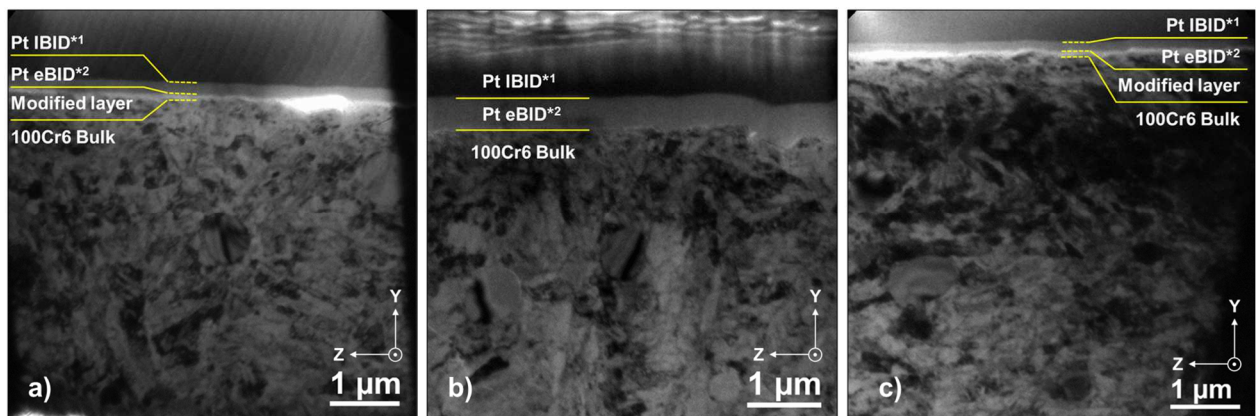
Because of stress and contact conditions, the layer could be caused by a reaction of grease elements with the bearing material (either with the third body particles or directly with the surface), or between themselves. To identify the layer morphology and depth, TEM analyses were conducted on the FIB lamellae.

3.2. TEM analysis

According to the XPS observation, the TEM analysis confirms the formation of a modified superficial layer on the surface of the inner ring raceway, for the lamella T1b-L and T2b-L, where the sliding ratio is high (Figure 6 a and c). On the other side no relevant layer can be observed on the lamella T1c (Figure 6 b).

Figure 6 shows a general overview of the lamella where, from up to down, the following layers can be detected:

- A first layer of platinum deposited using the FIB gallium ion beam, to protect the sample surfaces (Pt IBID^{*1} in Figure 6).
- A second layer of platinum deposited using the FIB electron beam (Pt eBID^{*2} in Figure 6). Using an electron beam, to fix the protective platinum layer, is less damaging for the sample surface than the ion beam but needs a longer deposition time.
- The modified layer, identified by the different brightness due to the lower density, regarding the steel. It is the superficial layer where the elements of the grease have been detected by XPS. This layer is observable in the T1b-L and T2b-L lamellae, but is not identifiable in the T1c-L lamella.
- The bulk of the bearing raceway, i.e., the matrix of the 100Cr6 steel (100Cr6 Bulk in Figure 6). Both grain refining and unclear nodule edges can be observed when approaching the surface, which is a classical TTS observed in surfaces under extreme contact conditions.



*1 Platinum ionic beam-induced deposition of Platinum

*2 Platinum electron beam-induced deposition of Platinum

Figure 6: Low magnification (x1,500) TEM observations in bright field of the three lamellae nano-machined in the traces T1 and T2. The chemical contrast reveals a white superficial layer, between the 100Cr6 bulk and the Pt eBID protection on the lamellae T1b-L and T2c-L, in the reversing points of T1 and T2, respectively.

Figure 7 shows a TEM image of the T1b-L lamella, taken at higher magnification. The modified layer can clearly be observed between the bearing raceway and the Pt eBID layer (Figure 7, a). Its thickness is measured to range between about 50 and 70 nm. Having resisted the hard cleaning protocol in the previous section and the vacuum conditions in the TEM, this layer presents a solid behavior with no volatile compounds. The higher gray level in the TEM images indicates that it has a density lower than bulk 100Cr6.

A deeper investigation of this superficial layer shows further stratification (Figure 7, b). An interface film, of a constant size of about 5 nm, is observed at the interface with bulk steel. Then, there is a larger layer ranging from about 35 to 60 nm thickness, which is an amorphous phase where crystalline nanoparticles are dispersed. A last stratum of thickness from about 7 to 20 nm, without crystalline nanoparticles, is observed at the surface extreme.

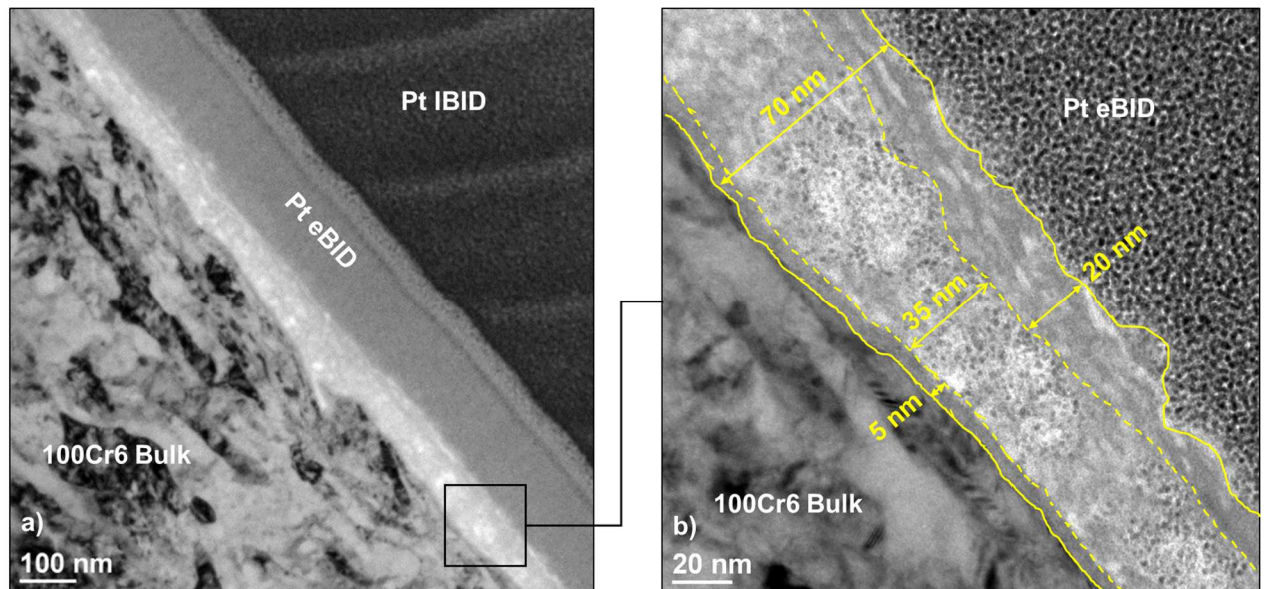


Figure 7: High magnification (x60,000) TEM observations in the bright field of the lamella T1b-L. A modified layer is fixed on the 100Cr6 bulk with a homogeneous depth ranging between 50 and 70 nm along the lamella. At the highest magnification, from the bulk to the Pt eBID layer, we can observe a thin interface layer; a larger amorphous phase containing nanoparticles; and a last amorphous layer.

For the lamella T1c-L, no consistent smoothed modified layer was observed in the surface using SEM. TEM observations at high magnification suggest an extremely thin layer of a thickness between about 6 and 15 nm (Figure 8), and this thin modified layer is not clearly identifiable along this lamella.

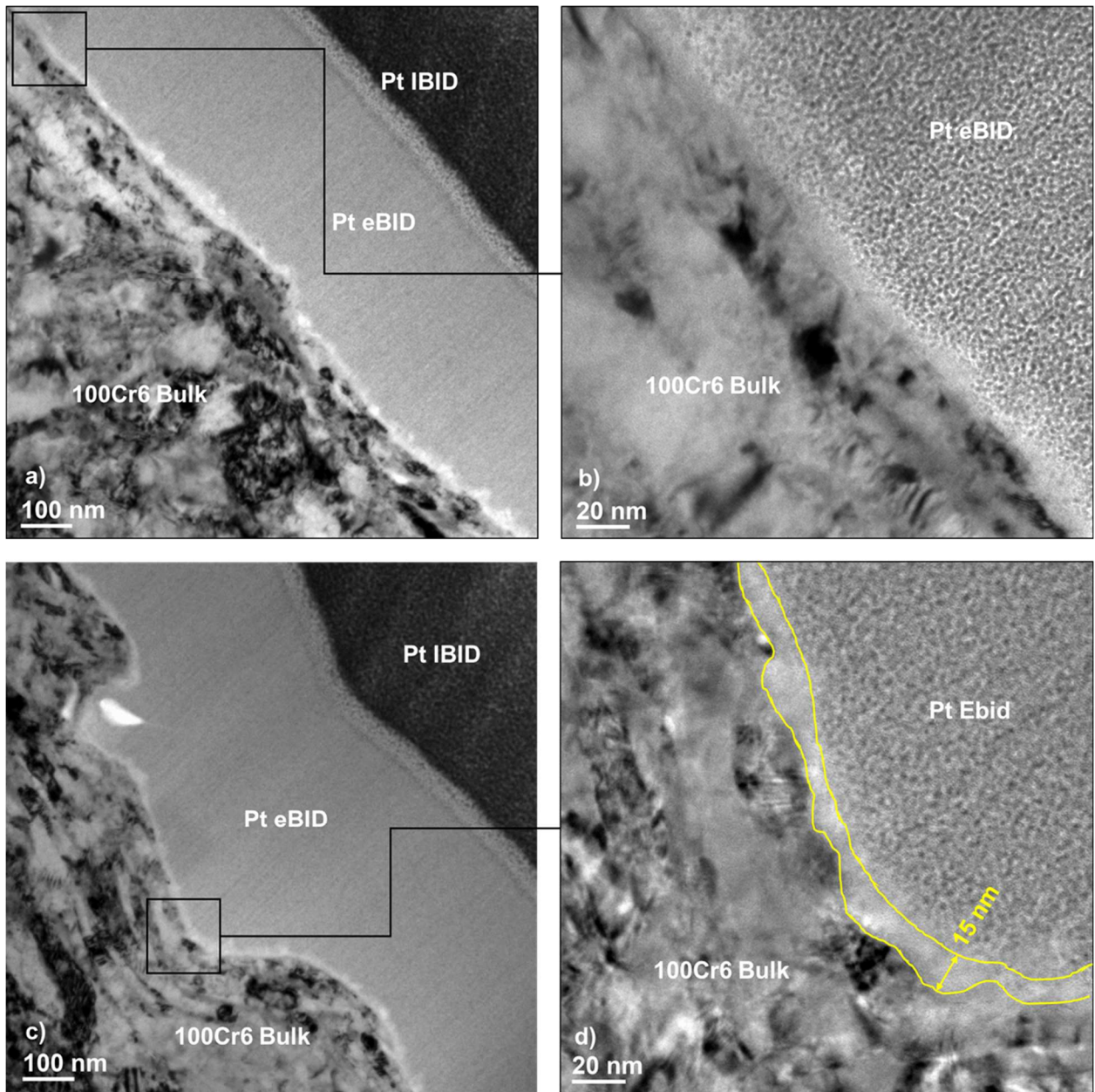


Figure 8: High magnification (x60,000) TEM observations in the bright field of the lamella T1C-L at two points along the FIB lamellae. A thin modified layer is fixed along the 100Cr6 bulk with a homogeneous depth about 6 nm along the lamella. At the highest magnification, the layer appears to not be developed in the b) section, whereas it is definable on the d) section.

Finally, the observations made on the lamella T2b-L show a modified layer of a thickness between about 100 and 205 nm, like the one detected in T1b-L (Figure 9, a). Like in T1b-L, the contrast of the identified layer with the bulk 100Cr6 steel is important, implying a different composition. The same stratification of the layer is also found (Figure 9, b). From the bulk 100Cr6 steel to the top, an interface film of thickness about 15 to 45 nm is observed. Then a 90 to 190 nm layer follows, which appears like an amorphous layer with dispersed crystalline nanoparticles inside.

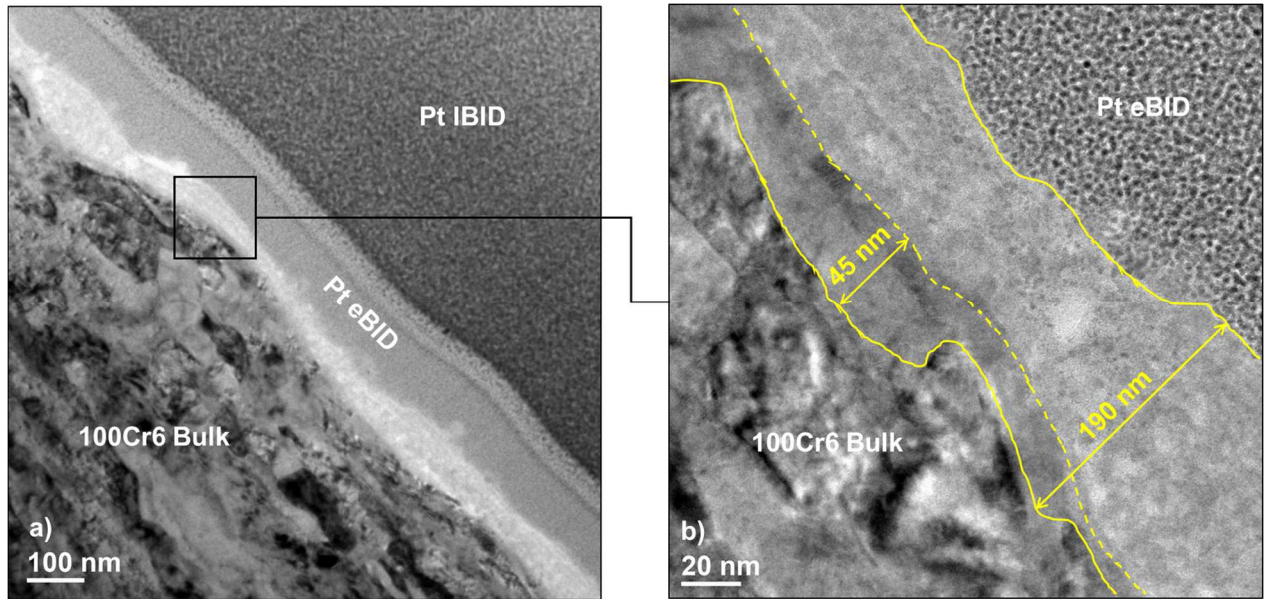


Figure 9: High magnification (x60,000) TEM observations in the bright field of the lamella T2b-L. A modified layer is fixed along the 100Cr6 bulk with a homogeneous depth about 100 to 205 nm along the lamella. At the highest magnification, from the bulk to the Pt eBID layer, an interface layer is observable, followed by a larger amorphous phase containing nanoparticles.

TEM analysis confirms a modified layer on the 100Cr6 contact surface, in the locations where a smooth superficial layer was observed by SEM [2]. Still, the layer morphology and thickness depend on the location of the surface sample.

A deep stratified modified layer develops where third body particles accumulate and a high sliding ratio is important, resulting in higher shearing at the contact surface. This is the case for the samples T1b-L and T2b-L, at the reverse point of B1 and B2, respectively. Mild wear may create many free chemical bonds, which react with the additives. Then, shearing applied on the third body, comprising grease and wear particles, can lead to developing a stratified layer.

For the sample T1c-L, where rolling motion predominates, only a thin interface layer is found. The unclear demarcation with bulk 100Cr6 steel implies that only the layer formed between the grease and the free chemical bonds is developed. This thin superficial layer may be thermally activated during the friction test. In contrast to the samples T1b-L and T1c-L, there is no additional stratification. This could be explained either by the lower superficial shear stress or by the lack of grease and third body particles found at the contact.

The reported observations highlight that a thin film is formed on the surface of the 100Cr6 raceway. The same grease elements are detected by XPS on the three selected areas. However, the availability of a third body, close to the contact and the local sliding (high shear stress), appears to promote the formation of a deeper modified layer. The composition and

stratification of this modified layer, resulting from an interaction between the grease components and the surface, depend on the local contact conditions and play a key role in accommodating contact and preventing quick superficial failures.

Conclusions

High loaded oscillating bearings show a long lifetime and stability over oscillating cycles with grease lubrication applied, even if extreme boundary conditions do not allow the establishment of a lubrication film. Previous studies evidenced topographical modifications of the raceway surface, obtained only for specific greases, which appear to protect and stabilize the contact interface. The aim of this study was to identify the morphology and thickness of this modified superficial layer, under such extreme operational conditions.

First, a commercial bearing, greased with a classic aeronautical lubricant, was prepared, and tested on a test bench dedicated to reproducing high loaded oscillating movements. Superficial observations of the inner ring raceway were conducted to highlight the transformation of the morphology of high-solicited areas. Then, specific surface zones, showing the modified morphology or not, were analyzed using XPS and showed grease elements on the raceway surface. Finally, the fabrication of FIB lamellae helped analyze sectional views of the surface and subsurface of the identified contact zones.

The main outcomes from the analysis are:

- Despite aggressive cleaning protocols, some chemical compounds of the lubricant were detected on the surface of the raceway. This implies a superficial layer over the steel substrate, probably raised from high reactive additive molecules reacting with the fresh steel surface at the initiation of the wear process.
- The observations of the FIB lamellae revealed that a modified layer is formed on the surface of the raceway, with a structure and composition different from the 100Cr6 steel substrate.
- The thickness and the stratification of the layer depend on the localization of the observed surface sample. An important sliding ratio may lead to a stronger development of the modified layer, because of free steel chemical bonds and possible heat localization to trigger reactions. An accumulation of grease and third body (wear) particles, available close to the contact zone, may have an influence on the formation of the modified layer.

Considering these findings, future studies will focus on the chemical composition of the modified layer to understand its establishment and its sustainability.

Declaration of competing interest

The authors declare that they have no known competing financial interests or personal relationships that could have appeared to influence the work reported in this paper.

Credit authorship contribution statement

L. Frache: Investigation, Methodology, Visualization, Conceptualization, Data curation, Writing - original draft. **E. Houara Komba:** Investigation, Methodology, Conceptualization, Data curation. **D. Philippon:** Methodology, Formal analysis, Supervision, Writing - review & editing. **N. Bouscharain** Methodology, Formal analysis, Supervision, Writing - review & editing. **J. Galipaud** XPS measurements, Formal analysis, Investigation. **T. Douillard** TEM analyzes, Formal analysis, Investigation. **K. Masenelli-Varlot:** Formal analysis, Writing - review & editing. **Y. Maheo:** Conceptualization, Funding acquisition. **F. Massi:** Methodology, Formal analysis, Supervision, Conceptualization, Writing - review & editing. **M.I De Barros:** XPS measurements, Formal analysis, Investigation. **Y. Berthier:** Conceptualization. **B. Bou-Said:** Supervision.

Acknowledgments

The authors acknowledge the French National Association of Research and Technology (ANRT) for its support to this work through the CIFRE convention N. 2018/0992, and the Consortium Lyon Saint-Etienne de Microscopy (CLYM) for the access to the TEM microscope.

References

1. Harris T, Rumbarger JH, Butterfield CP. Wind Turbine Design Guideline DG03: Yaw and Pitch Rolling Bearing Life [Internet]. 2009 déc [cité 30 mars 2020] p. NREL/TP-500-42362, 969722. Report No.: NREL/TP-500-42362, 969722. Disponible sur: <http://www.osti.gov/servlets/purl/969722-YFwQR5/>
2. Komba EH, Massi F, Bouscharain N, Le Jeune G, Berthier Y, Maheo Y. Experimental damage analysis in high loaded oscillating bearings. *Tribol Int.* oct 2016;102:507-15.
3. El-Thalji I, Jantunen E. A descriptive model of wear evolution in rolling bearings. *Eng Fail Anal.* oct 2014;45:204-24.
4. Halme J, Andersson P. Rolling contact fatigue and wear fundamentals for rolling bearing diagnostics - state of the art. *Proc Inst Mech Eng Part J J Eng Tribol.* avr 2010;224(4):377-93.
5. Gegner J. Tribological Aspects of Rolling Bearing Failures. In: Kuo C-H, éditeur. *Tribology - Lubricants and Lubrication* [Internet]. InTech; 2011 [cité 19 juin 2020]. Disponible sur: <http://www.intechopen.com/books/tribology-lubricants-and-lubrication/tribological-aspects-of-rolling-bearing-failures>
6. Denape J. Third Body Concept and Wear Particle Behavior in Dry Friction Sliding Conditions. *Key Eng Mater.* mars 2015;640:1-12.
7. Olofsson U, Andersson S, Björklund S. Simulation of mild wear in boundary lubricated spherical roller thrust bearings. *Wear.* juill 2000;241(2):180-5.
8. Morales-Espejel GE, Brizmer V. Micropitting Modelling in Rolling–Sliding Contacts: Application to Rolling Bearings. *Tribol Trans.* juill 2011;54(4):625-43.
9. Nierlich W, Gegner J. MATERIAL RESPONSE MODELS FOR SUB-SURFACE AND SURFACE ROLLING CONTACT FATIGUE. :11.
10. Sadeghi F, Jalalahmadi B, Slack TS, Raje N, Arakere NK. A Review of Rolling Contact Fatigue. *J Tribol.* 1 oct 2009;131(4):041403.
11. Massi F, Bouscharain N, Milana S, Le Jeune G, Maheo Y, Berthier Y. Degradation of high loaded oscillating bearings: Numerical analysis and comparison with experimental observations. *Wear.* sept 2014;317(1-2):141-52.
12. Jiang Y, Sehitoglu H. A model for rolling contact failure. *Wear.* janv 1999;224(1):38-49.
13. Olver AV. The Mechanism of Rolling Contact Fatigue: An Update. *Proc Inst Mech Eng Part J J Eng Tribol.* mai 2005;219(5):313-30.
14. Kotzalas MN, Harris TA. Fatigue Failure Progression in Ball Bearings. *J Tribol.* 1 avr 2001;123(2):238-42.
15. Warhadpande A, Sadeghi F, Kotzalas MN, Doll G. Effects of plasticity on subsurface initiated spalling in rolling contact fatigue. *Int J Fatigue.* mars 2012;36(1):80-95.
16. Beckman M. Back and forth with oscillating bearings. *Tribol Lubr Technol.* juin 2020;76(6):48-52.

17. Ghezzi I, Houara Komba EW, Tonazzi D, Bouscharain N, Jeune GL, Coudert J-B, et al. Damage evolution and contact surfaces analysis of high-loaded oscillating hybrid bearings. *Wear*. juill 2018;406-407:1-12.
18. Cavacece F, Frache L, Tonazzi D, Bouscharain N, Philippon D, Le Jeune G, et al. Roller bearing under high loaded oscillations: Life evolution and accommodation mechanisms. *Tribol Int*. juill 2020;147:106278.
19. Tonazzi D, Komba EH, Massi F, Le Jeune G, Coudert JB, Maheo Y, et al. Numerical analysis of contact stress and strain distributions for greased and ungreased high loaded oscillating bearings. *Wear*. avr 2017;376-377:1164-75.
20. Busquet M, Descartes S, Berthier Y. Formation conditions of mechanically modified superficial structures for two steels. *Tribol Int*. déc 2009;42(11-12):1730-43.
21. Sauger E, Fouvry S, Ponsonnet L, Kapsa P, Martin JM, Vincent L. Tribologically transformed structure in fretting. *Wear*. oct 2000;245(1-2):39-52.
22. Eleöd A, Baillet L, Berthier Y, Törköly T. Deformability of the near surface layer of the first body. In: *Tribology Series* [Internet]. Elsevier; 2003 [cité 22 juin 2020]. p. 123-32. Disponible sur: <https://linkinghub.elsevier.com/retrieve/pii/S0167892203801256>
23. Minfray C, Martin JM, Esnouf C, Le Mogne T, Kersting R, Hagenhoff B. A multi-technique approach of tribofilm characterisation. *Thin Solid Films*. janv 2004;447-448:272-7.
24. Philippon D, De Barros-Bouchet M-I, Le Mogne Th, Lerasle O, Bouffet A, Martin J-M. Role of nascent metallic surfaces on the tribochemistry of phosphite lubricant additives. *Tribol Int*. juin 2011;44(6):684-91.
25. Righi MC, Loehlé S, De Barros Bouchet MI, Mambingo-Doumbe S, Martin JM. A comparative study on the functionality of S- and P-based lubricant additives by combined first principles and experimental analysis. *RSC Adv*. 2016;6(53):47753-60.
26. Heuberger R, Rossi A, Spencer ND. Pressure Dependence of ZnDTP Tribochemical Film Formation: A Combinatorial Approach. *Tribol Lett*. 27 sept 2007;28(2):209-22.
27. Burbank J, Woydt M. Friction and wear reductions in slip-rolling steel contacts through pre-conditioned chemical tribofilms from bismuth compounds. *Wear*. août 2016;360-361:29-37.
28. Hart RT, Kerr AA, Eckert NA. Bismuth Sulfide (Bi_2S_3) as the Active Species in Extreme Pressure Lubricants Containing Bismuth Carboxylates and Sulfur Compounds. *Tribol Trans*. 23 déc 2009;53(1):22-8.
29. Rohr O. Bismuth – the new ecologically green metal for modern lubricating engineering. *Ind Lubr Tribol*. août 2002;54(4):153-64.
30. Wan GTY, Lankamp H, de Vries A, Ioannides E. The Effect of Extreme Pressure (EP) Lubricants on the Life of Rolling Element Bearings. *Proc Inst Mech Eng Part J J Eng Tribol*. 1 déc 1994;208(4):247-52.
31. Ji X, Chen Y, Zhao G, Wang X, Liu W. Tribological Properties of CaCO_3 Nanoparticles as an Additive in Lithium Grease. *Tribol Lett*. janv 2011;41(1):113-9.

32. Spikes H. The History and Mechanisms of ZDDP. Tribol Lett. oct 2004;17(3):469-89.
33. Rudnick LR. Lubricant Additives. :796.
34. THE AEROSHELL BOOK [Internet]. 19^e éd. 2012. (Shell Aviation). Disponible sur:
<https://www.shell.com/business-customers/aviation/aeroshell/knowledge-centre/the-aeroshell-book.html>